Select Liquefaction Case Histories from the 2001 Nisqually, Washington Earthquake: A Digital Dataset and Assessment of Model Performance

Ryan A. Rasanen, M.EERI, Mertcan Geyin, and Brett W. Maurer, M.EERI

While soil liquefaction is common in earthquakes, the case history data required to train and test state-of-practice prediction models remains comparatively scarce, owing to the breadth and expense of data that comprise a single case history. The 2001 Nisqually, Washington, earthquake, for example, occurred in a metropolitan region and induced damaging liquefaction in the urban cores of Seattle and Olympia, yet case history data has not previously been published. Accordingly, this paper compiles 24 cone-penetration-test (CPT) case histories from free-field locations. The many methods used to obtain and process the data are detailed herein, as is the structure of the digital dataset. The case histories are then analyzed by 18 existing liquefaction response models to determine whether any is better, and to compare model performance in Nisqually against global observations. While differences are measured, both between models and against prior global case histories, these differences are often statistically insignificant considering finite-sample uncertainty. This alludes to the general inappropriateness of championing models based on individual earthquakes or otherwise small datasets, and to the ongoing needs for additional case history data and more rigorous adherence to best practices in model training and testing.

Introduction

The 28 February 2001 M_w6.8 Nisqually, Washington, earthquake damaged infrastructure throughout the Puget Sound Region of the U.S. Pacific Northwest. This included damage due to soil liquefaction, which was concentrated in Holocene alluvium and artificial fills in the urban

a) Department of Civil and Environmental Engineering, University of Washington

b) Norwegian Geotechnical Institute

areas of Olympia and Seattle (e.g., Bray et al., 2001; Seattle Office of Emergency Management, 2019). Intraslab earthquakes associated with the Cascadia Subduction zone, such as the 2001 Nisqually earthquake, are a common occurrence deep beneath the Puget Sound. Prior to the 2001 event, M_w7.1 and M_w6.7 ruptures occurred in 1949 and 1965, respectively, causing widespread ground failures (Chleborad and Shuster, 1990), often in areas where liquefaction was again observed in 2001. But unlike these prior events, the most recent was recorded by a dense network of strong motion stations across the affected region and occurred at a time in which in-situ geotechnical tests were commonplace. Although manifestations of liquefaction, or the lack thereof, were documented by reconnaissance teams in 2001, liquefaction case histories from the event have not been published.

While several "tiers" of liquefaction prediction model exist, including "geospatial" (e.g., Zhu et al., 2017; Rashidian and Baise, 2020; Geyin et al., 2021), "semi-empirical stress based" (e.g., Robertson and Wride, 1998; Moss et al., 2006; Boulanger and Idriss, 2016), and "constitutive, fully mechanistic" (e.g., Boulanger and Ziotopoulou, 2015), the second of these is the most common in routine practice. All models within this tier are based on the same modeling framework originally proposed by Seed and Idriss (1971) and Whitman (1971). This framework is semi-empirical in that the soil's resistance to liquefaction is correlated to an in-situ geotechnical test measurement, which foremost serves as a proxy of soil density. Among the in-situ tests for which models have been developed, the cone penetration test (CPT) is widely perceived to offer important advantages (NRC, 2016). The training of a CPT-based liquefaction triggering model requires several types of field data that collectively form a "case history." These include: (i) observations of liquefaction, or the lack thereof, which are almost always made at the ground surface; (ii) a profile of CPT data from the site of observation; (iii) knowledge of the groundwater table (*GWT*) depth, both at the time of the earthquake and at the time of CPT testing; and (iv) knowledge of the peak ground acceleration (*PGA*) at the site.

Owing to the breadth and expense of these data, liquefaction case histories have remained relatively scarce. Aside from the 2010-2011 Canterbury sequence, from which a large quantity of data was compiled in the city of Christchurch (e.g., Geyin et al., 2021), fewer than 300 high quality CPT case histories have been compiled from all other global earthquakes combined (e.g., Boulanger and Idriss, 2016). The lack of data from a wide variety of seismologic, geologic, and geomorphic settings inherently constrains the development of better prediction models, given the

semi-empirical nature of the "stress-based" framework. The absence of case-history data from a 21st-century earthquake in a major U.S. city is especially notable, given that case histories have been compiled from relatively rural settings without many seismic instruments, and from events that predate modern reconnaissance tools and the CPT itself. Accordingly, this paper compiles a digital dataset of 24 CPT-based liquefaction case histories from the Nisqually earthquake. The cases are compiled from the free field on ground that is generally level, and the data is provided in a widely accessible format. These cases are among very few associated with subduction zone earthquakes, and potentially the only cases from an intraslab rupture. This compilation is also the second largest from any U.S. earthquake and the fourth largest from any earthquake outside of Canterbury, New Zealand. Only the 1989 Loma Prieta (U.S), 1999 Chi-Chi (Taiwan), and 2012 Emilia (Italy) earthquakes have produced more CPT case histories to date. Moreover, the newly compiled cases are from a region underlaid by unusually deep sedimentary basins, with $Z_{1.0}$ values (i.e., depths to a shear-wave velocity of 1 km/s) exceeding 800 m. The Nisqually case histories thus provide a useful addition for model training and testing. Following compilation and discussion of these new cases, the data are used to test the efficacies of 18 existing liquefaction response models that predict the triggering and manifestation of liquefaction. These results are compared to prior analyses of global cases to preliminarily assess whether, and how, model performance differs for the Nisqually dataset.

The paper is presented in two parts. The first pertains to the compilation of liquefaction case histories from the 2001 Nisqually earthquake. The various methods used to process and populate the database are detailed, as are the structure and formatting of the resulting dataset. The second pertains to the performance evaluation of eighteen popular liquefaction response models using the newly compiled case histories.

Compilation of Case Histories

Twenty-four liquefaction case histories are herein compiled from the 2001 Nisqually earthquake, which was epicentrally located in the vicinity of the Nisqually River's confluence with the Puget Sound, and which had an estimated depth to top of rupture (Z_{TOR}) of 50 km (e.g., Bustin et al., 2004). The event was recorded by a network of more than 60 strong ground-motion stations located within 100 km of the fault rupture. A regional overview of the case-history sites, ground-motion recording stations, and location of fault rupture is shown in Figure 1. Of the 24 case-history sites,

17 map to artificial fills and the remainder are generally in Holocene alluvium (Washington Division of Geology and Earth Resources, 2016). Of relevance to the development of "magnitude-bound" relationships (e.g., Rasanen et al., 2021), the most distal observation of liquefaction had an epicentral, Joyner Boore, and rupture distance of $R_{EPI} = 74$ km, $R_{JB} = 73$ km, and $R_{RUP} = 90$ km, respectively. A succinct summary of the compiled case histories is given in Table 1. The details presented therein, in addition to many others, are discussed subsequently, and an extended version of the table is provided in the appendix.

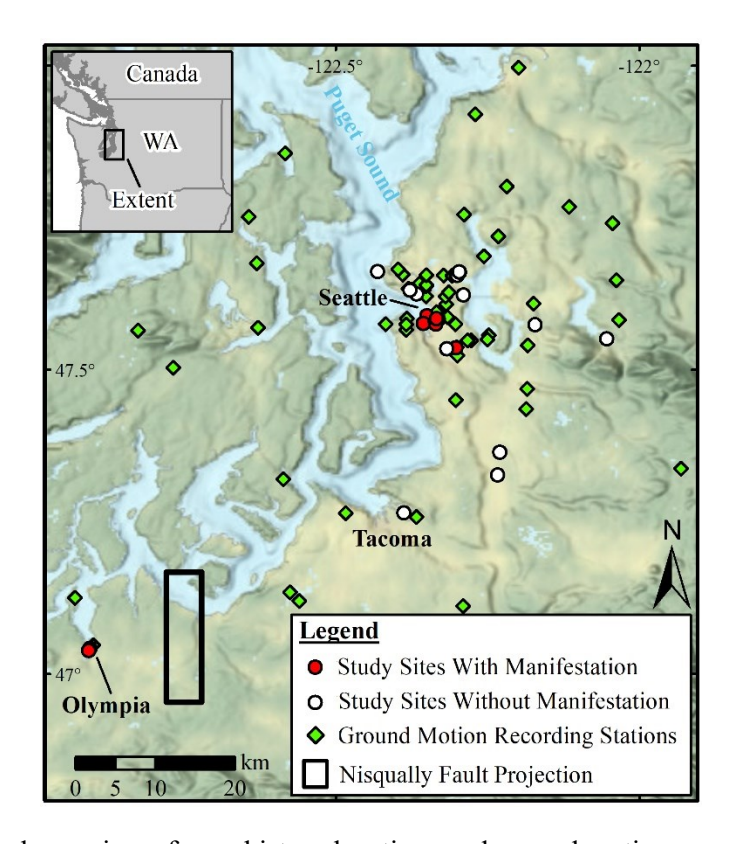


Figure 1. Regional overview of case-history locations and ground motion recording stations.

Liquefaction Response

Case histories were compiled with emphasis on free-field level-ground sites. Nine of the twenty-four case history sites are herein classified as "positive," meaning that surficial manifestations of liquefaction were observed. These consisted of: (i) seven sites with varying amounts of liquefaction ejecta, and in some cases, ground cracks and perceptible vertical settlements; (ii) one site (Capitol Lake-02) having both traces of liquefaction ejecta and a crack with ~5 cm of horizontal displacement, suggesting the possibility of minor lateral spreading toward a nearby lake;

and (iii) one site (SODO-02) that lacked ejecta, but where cracks and differential settlements were observed in pavements and sidewalks on the perimeter of an improved area. The remaining fifteen sites are classified as "negative," meaning that no surficial evidence of liquefaction was observed. In general, these latter sites are heavily trafficked, high visibility locations where focused reconnaissance efforts failed to identify any evidence of liquefaction from observations of the ground surface, pavements, infrastructure, etc. In each of these cases, CPTs and borings suggest the presence of soils susceptible to liquefaction and estimated ground motions (discussed subsequently) were sufficient to trigger liquefaction in soils with low cyclic resistance (e.g., de Magistrals, 2013). In addition, a large majority of the case-history sites – both with and without manifestations – are locations where ground failures were previously observed in the 1949 and/or 1965 earthquakes, as documented by Chleborad and Schuster (1990). Sources of reconnaissance information included Bray et al. (2001), Seattle Office of Emergency Management (2019), Pacific Northwest Seismic Network (2001), Hausler and Koelling (2004), Walsh (2001), Geoengineers, Inc. (2003), and personal records and communication with individuals from the City of Seattle, regional utility companies, the University of Washington, and those who previously published reconnaissance reports in the public domain. The imbalance of negative over positive cases is judged to be appropriate. While historical sampling practices have produced datasets that are heavily biased towards positives, such datasets do not accurately represent the population of field observations, wherein liquefaction is typically observed at a small fraction of sites where susceptible soils are present.

Table 1. Summary of compiled case histories. An extended version appears in the appendix.

No.	Site Name	Longitude (WGS84)	Latitude (WGS84)	GWT Depth (m)	Manifestation	Conditional Median PGA (g)	Conditional Lognormal o of PGA
1	Capitol Lake-01	-122.904273	47.041971	0.61	Yes	0.221	0.192
2	SODO-01	-122.330874	47.582869	3.05	Yes	0.234	0.079
3	Capitol Lake-02	-122.906716	47.038174	1.52	Yes	0.217	0.224
4	Harbor Island-01	-122.349801	47.588704	3.29	Yes	0.180	0.144
5	Harbor Island-02	-122.355378	47.575863	2.44	Yes	0.184	0.167
6	SODO-02	-122.335805	47.578781	2.13	Yes	0.199	0.145
7	SODO-03	-122.334837	47.575020	2.74	Yes	0.198	0.164
8	SODO-04	-122.333936	47.584171	0.99	Yes	0.197	0.099
9	Boeing Field-01	-122.301620	47.536125	2.13	Yes	0.201	0.100
10	Duwamish-01	-122.316733	47.534451	2.29	No	0.192	0.188
11	Discovery Park-01	-122.430819	47.661330	3.96	No	0.084	0.244
12	Elliott Ave-01	-122.366639	47.624508	1.83	No	0.142	0.142
13	Smith Cove-01	-122.376982	47.631682	2.74	No	0.127	0.120
14	Smith Cove-02	-122.377416	47.630920	3.66	No	0.128	0.123
15	Emerald Downs-01	-122.232961	47.327071	1.00	No	0.158	0.353
16	Bush School-01	-122.289623	47.622844	3.05	No	0.119	0.205
17	Factoria-01	-122.171810	47.573752	1.52	No	0.102	0.245
18	UW-01	-122.301101	47.654810	0.76	No	0.129	0.156
19	UW-02	-122.299341	47.655123	0.76	No	0.129	0.166
20	UW-03	-122.295665	47.660272	2.44	No	0.127	0.189
21	UW-04	-122.296197	47.660901	2.44	No	0.126	0.190
22	Issaquah-01	-122.053685	47.550644	2.44	No	0.125	0.279
23	Blair Waterway-01	-122.387559	47.264867	3.05	No	0.104	0.236
24	Green River-01	-122.229279	47.364461	5.18	No	0.166	0.335

Subsurface Data

Case histories were compiled utilizing existing geotechnical tests available in the Jeschke et al. (2019) database, which presently contains more than 100,000 subsurface tests and observations from Washington State, including CPTs, standard penetration tests (SPTs), borings, shear-wave velocity (V_S) measurements, laboratory tests, and well logs. While significantly more CPT case-histories could potentially be compiled from the Nisqually earthquake, the reliance on existing tests in the present effort resulted in 24 sites where the liquefaction response was reliably documented in 2001. A future effort could compile additional case histories, particularly cases based on SPTs, which in the Jeschke et al. (2019) database greatly outnumber CPTs in the affected

region. Moreover, these data collectively form the basis for a very large case-history compilation whenever a large earthquake next impacts the region. In compiling case histories, CPTs for which the pre-drill depth exceeded the GWT depth were excluded, given the additional uncertainty associated with such cases. For the remaining cases, CPT data were infilled in the pre-drill zone by averaging the data measured over a 10 cm interval beneath the depth of pre-drill and applying that average uniformly to the pre-drill interval. In the absence of this correction, the recorded data is that of noise as the cone penetrates the open boring. The purpose of this correction, which results in each CPT having an initial series of repeating measurements, is simply to provide reasonable data for approximating soil unit weights and in-situ stresses below the pre-drill zone, should analysts estimate unit weights via CPT correlations. It should thus be understood that data above the reported pre-drill depth is not an actual measurement. Cross-correlation (Buck et al., 2002) was used to ensure that tip and sleeve measurements were properly aligned in accordance with ASTM D5778. For 15 of the 24 CPTs, pore pressure measurements (u₂) are available, and in these cases, the reported cone tip resistance is q_t (i.e., corrected for u₂ effects). Analysts should therefore not make additional corrections when u₂ is provided. For the remainder of CPTs without u₂ measurements, the reported cone tip resistance is q_c. This discrepancy (i.e., combining q_c and q_t measurements) has historically been ignored in liquefaction modeling, given that u₂ measurements are often unavailable and that u₂ effects are negligible in soils susceptible to liquefaction. GWT levels were sourced from the geotechnical reports that documented CPTs while also considering proximal borings, well logs, and monitoring wells. In general, multiple GWT measurements were available in the immediate vicinity of each case-history site. For case histories where surface manifestations were observed, CPTs were typically performed within 10-20 m of the observed sand boil or spreading crack, and occasionally much closer. This is consistent with the methodology adopted by Geyin et al. (2021) to classify case histories in New Zealand and is believed to be consistent with case histories elsewhere, although many authors have not disclosed the locations of in-situ tests relative to liquefaction observations. Nonetheless, and like all liquefaction case histories, it is possible that CPTs do not well represent the subsurface profiles that gave rise to the observed responses. CPTs might differ from these "true" CPTs due to measurement errors or subsurface spatial variability, or because the surficial manifestation was produced by soil that liquefied at some lateral distance from the manifestation, and not directly beneath it (e.g., Bassal and Boulanger, 2021). Thus, the classified manifestation is itself uncertain, just as with any other case history.

Ground Motion Intensities (PGAs)

The Nisqually earthquake was recorded by at least 60 strong-motion records having $R_{RUP} < 100$ km. On average, the 24 case-history sites are located 1.9 km from the nearest station, with 13 sites located within 1 km of a recording. Inherent to the stress-based framework for predicting liquefaction, the imposed cyclic stress is computed from PGA, and thus, all such existing models use this intensity measure (IM). While future liquefaction response models may use IMs other than PGA, or vector IMs that utilize multiple measures of intensity, PGA continues to be among the most efficient, sufficient, and predictable IMs for the initiation of liquefaction (e.g., Sideras, 2019; Wu et al. 2022). Considering this, and that IMs other than PGA have not been estimated for many prior case histories, it is unlikely that PGA will be supplanted in the very near future.

For the Nisqually earthquake, PGAs were estimated at case-history sites using the approach implemented by Bradley (2014) in Canterbury, New Zealand, which has since been used in numerous analyses of Canterbury liquefaction (e.g., Maurer et al., 2015a; Geyin and Maurer, 2021; Rateria and Maurer, 2022). Using this approach, a "conditional" distribution of PGA is computed at any given site, wherein predictions from a ground-motion model (GMM), which provides the unconditional distribution, are conditioned on ground-motion stations (SMS). In effect, instrumental PGAs and GMM predictions are merged considering site conditions at SMS locations and case-history sites, as well as the spatial correlation of intra-event residuals. Our implementation is analogous to that in Canterbury, except that models appropriate for the Cascadia Subduction Zone are adopted. The PGAs at any SMS, i, may be expressed as:

$$\ln (PGA_i) = \mu_{\ln PGA_i} + \eta + \varepsilon_i, \tag{1}$$

where $\ln(PGA_i)$ is the natural logarithm of the observed PGA at SMS i; $\mu_{\ln PGA_i}$ is the mean of the natural logarithm of PGA at SMS i predicted by a GMM, which is a function of various site, path, and source parameters; η is the inter-event residual, which by definition is the same at all locations; and ε_i is the intra-event residual, which varies from site to site but is spatially correlated. Within Eq. 1, the GMM predicts a PGA distribution generically defined as:

$$\ln(PGA_i) \sim N(\mu_{\ln PGA_i}, \sigma_{\eta}^2 + \sigma_{\varepsilon}^2), \tag{2}$$

where $X \sim N(\mu_X, \sigma_X^2)$ indicates that X has a normal distribution with mean, μ_X , and variance, σ_X^2 . With knowledge of PGA, η , and ε at SMS sites, conditional PGA distributions can be computed at the locations of liquefaction case histories.

First, the Kuehn et al. (2020) subduction zone GMM, which has Cascadia regional adjustment factors, was used to compute unconditional PGA distributions at approximately 70 SMS sites in the Puget Sound region. SMS records from dams and those elevated in buildings were first removed. The Kuehn et al. (2020) GMM was implemented for an $M_w6.8$ Cascadia intraslab rupture, with R_{RUP} computed from a strike of 360°, dip of 70°, and Z_{TOR} of 50 km based on Bustin et al. (2004), Ichinose et al. (2004), and Kao et al. (2008). Regional basin flags were assigned as mapped in Ahdi et al. (2020) and Parker et al. (2020), except for the Seattle basin, for which the updating of Wirth et al. (2018) was used. $Z_{I.0}$ and the depth to a V_S of 2500 m/s ($Z_{2.5}$) were computed from the Stephenson et al. (2017) regional velocity model. Lastly, for a large majority of SMS sites, the time-averaged V_S over the upper 30 m (V_{S30}) was adopted from the site-specific measurements of Wong et al. (2011) or McPhillips et al. (2020). For the remainder, and for most case-history sites, V_{S30} was assigned from the region-specific map of Palmer et al. (2007). Site-specific GMM inputs are provided in Table S1 for each case-history site.

A mixed-effects regression was next used to compute η and the ε_i 's for each SMS (e.g., Pinheiro et al., 2008). The covariance matrix of intra-event residuals was then computed by accounting for the spatial correlation between SMS locations and a test site of interest. In this regard, the joint distribution of intra-event residuals at a site of interest and the SMS is:

$$\begin{bmatrix} \varepsilon^{site} \\ \varepsilon^{SMstation} \end{bmatrix} = N \begin{pmatrix} \begin{bmatrix} 0 \\ \mathbf{0} \end{bmatrix}, \begin{bmatrix} \sigma_{\varepsilon^{site}}^2 & \Sigma_{12} \\ \Sigma_{21} & \Sigma_{22} \end{bmatrix} \end{pmatrix}, \tag{3}$$

where $X \sim N(\mu_X, \Sigma)$ indicates that X has a multivariate normal distribution with mean μ_X and covariance matrix Σ (i.e., similar to Eq. 2, but in vector form), and where $\sigma_{\varepsilon^{site}}^2$ is the variance of the intra-event residual at a case history site. The components of the covariance matrix were computed from:

$$\Sigma(i,j) = \rho_{i,j} \, \sigma_{\varepsilon i} \sigma_{\varepsilon j} \tag{4}$$

where $\rho_{i,j}$ is the spatial correlation of intra-event residuals between locations i and j, and $\sigma_{\varepsilon i}$ and $\sigma_{\varepsilon i}$ are the standard deviations of the intra-event residual at those respective locations. This spatial

correlation was computed using the model of Goda and Atkinson (2009), which is specific to subduction zones. Based on the joint distribution of intra-event residuals (Eq. 3), the conditional distribution of ε ^{site} was computed (e.g., Johnson and Wichern, 2007):

$$\begin{split} \left[\varepsilon^{site} \middle| \varepsilon^{SMstation}\right] &= N(\Sigma_{12} \cdot \Sigma_{22}^{-1} \cdot \varepsilon^{SMstation}, \sigma_{\varepsilon^{Site}}^2 - \Sigma_{12} \cdot \Sigma_{22}^{-1} \cdot \Sigma_{21}) \\ &= N(\mu_{\varepsilon^{Site} \mid_{\varepsilon^{SMstation}}} \sigma_{\varepsilon^{Site} \mid_{\varepsilon^{SMstation}}}^2) \end{split} \tag{5}$$

Using the conditional distribution of $\varepsilon^{\text{site}}$ and substituting into Eq. 2, the conditional distribution of PGA at a case history site, PGA_{site} , is:

$$[ln PGA_{site} | ln PGA_{SMstation}] = N(\mu_{lnPGA_i} + \eta + \mu_{s}^{site} |_{sSMstation}, \sigma_{ssite}^{2} |_{sSMstation})$$
(6)

This conditional distribution is lognormal and defined by the conditional median and conditional uncertainty (i.e., lognormal standard deviation). When a case history is located far from an SMS, the conditional and unconditional distributions are more similar (i.e., the PGA distribution assigned to the site is similar to that predicted by the GMM). Conversely, when a case history is very near to an SMS, the conditional distribution of PGA approaches the recorded value. The conditional median and conditional uncertainty of PGA are provided in the dataset for each case history and are mapped for the Seattle area in Figures 2 and 3, respectively, where 17 of 24 case histories are located. The complete PGA distribution may be generated by:

$$PGA_x = PGA_{50} * \exp(n\sigma_{lnPGA}) \tag{7}$$

where PGA_x is the value of PGA for the x^{th} percentile of the conditional distribution, PGA_{50} is the conditional median, σ_{lnPGA} is the conditional lognormal standard deviation, and n is the "z-value" of the standard normal distribution for the x^{th} percentile. The 16^{th} and 84^{th} percentiles of the distribution, for example, are computed with n values of -1 and 1, respectively. While many prior compilations and analyses of liquefaction case histories (e.g., those training probabilistic triggering models) have assigned uncertainties to PGAs in a largely subjective manner, the adopted approach computes uncertainty explicitly and objectively. These advantages also apply to the estimates of median PGAs, which for other case histories have often been computed with less rigor and more subjectivity (e.g., assuming that the PGA at a site of interest is equal to that at the nearest recording station, despite potential differences in path and site effects).

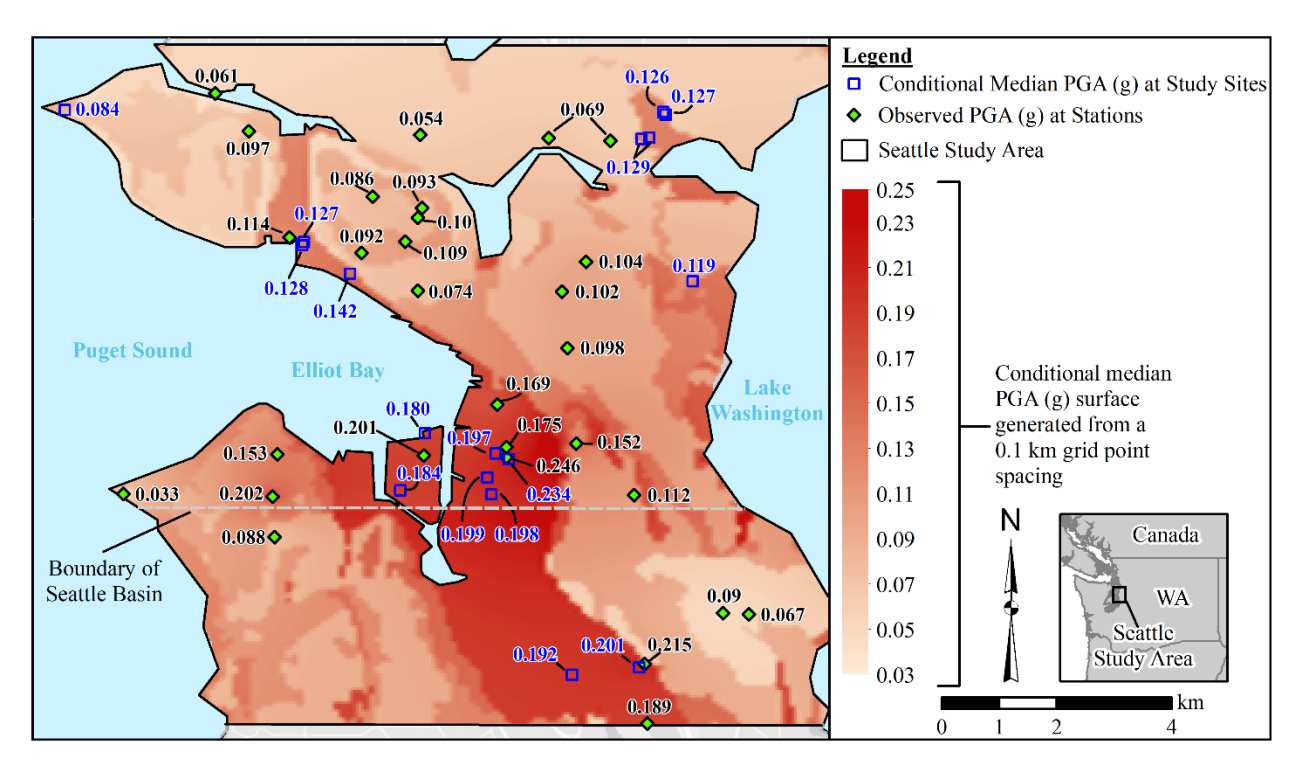


Figure 2. Recorded and computed conditional median *PGA*s in the Seattle area.

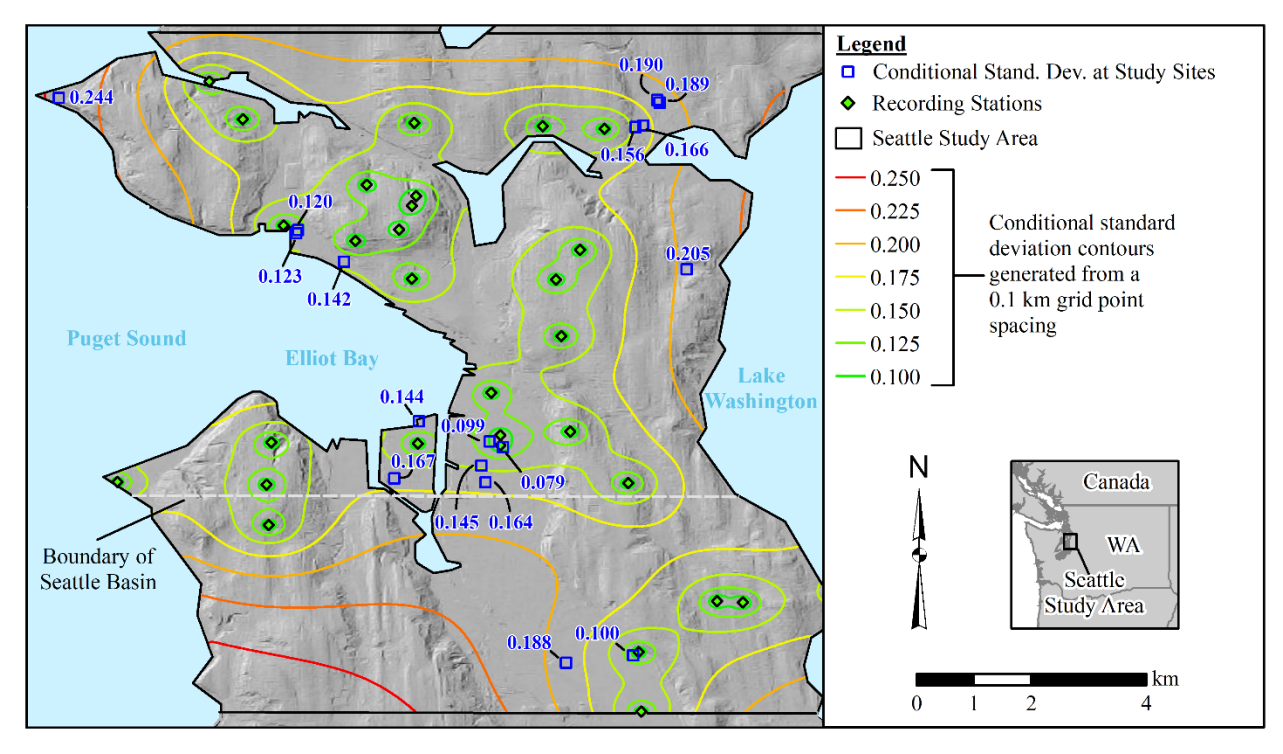


Figure 3. Computed conditional lognormal standard deviations of *PGA* in the Seattle area.

Data Structure

Provided in Table S1 of the appendix is a comprehensive summary of the case-history metadata. In addition to the data given in Table 1, Table S1 provides: citations for the geotechnical testing and post-earthquake reconnaissance; GMM inputs for each case-history site (e.g., V_{S30} , $Z_{1.0}$, $Z_{2.5}$, basin flags); notes and commentary specific to each case history; and the CPT pre-drill depth and test date. The CPT data for each case history is also provided in the appendix in 24 separate files (.xlsx format), where the most pertinent metadata specific to each case is again given (e.g., GWT and pre-drill depths, median and sigma of conditional PGA, etc.). The structure of each of these 24 files, which are named after our site identifiers (e.g., "Bush School-01.xlsx), is illustrated in Table 2 for case history No. 16. The dataset can also be accessed via this paper's appendix or the DesignSafe data depot at Rasanen et al. (2022) (https://doi.org/10.17603/ds2-nsf8-7944).

Table 2. Case-history data structure (shown is the data for case history 16: Bush School-01).

Depth (m)	q (MPa)	fs (MPa)	u ₂ (MPa)	Site Name	Bush School-01
0	2.208	0.090	0.000	Latitude (WGS84)	47.6228442
0.01	2.208	0.090	0.000	Longitude (WGS84)	-122.289624
0.02	2.208	0.090	0.000	Geotechnical Reference	ZZA, Inc. (2002)
0.03	2.208	0.090	0.000	Test Date	6/11/2002
0.04	2.208	0.090	0.000	Manifestation Classification	No
0.05	2.208	0.090	0.005	Water Table Depth (m)	3.05
•	•	•	•	Pre-drill (m)	0.61
•	•	•	•	Conditional Median PGA (g)	0.119
•	•	•	•	Conditional Standard Deviation	0.205

Limitations and Uncertainties

The methods used to compile Nisqually case histories are consistent with past precedent and, in some respects, are more rigorous (e.g., the measurement and estimation of ground motions). Nonetheless, and like existing case histories, there are limitations and uncertainties that analysts should be aware of. First, it is generally acknowledged that soil shear strength, as measured by penetration resistance, slowly increases with time (e.g., Kulhaway and Mayne, 1990), meaning that the time of in-situ testing relative to the time of the earthquake may be relevant. Despite this possibility, there has been no standard or best practice for the relative timing of in-situ testing when compiling case-history data. Inherent to existing compilations of global case histories (e.g.,

Boulanger and Idriss, 2016), in-situ testing has been performed both well in advance and well after the earthquake of interest, often with multiple other earthquakes occurring in the meantime. This issue is discussed in detail by Geyin et al. (2021). In the dataset compiled herein, CPTs were performed in advance of the Nisqually earthquake at 22 sites and approximately two years after the earthquake at the remaining two sites. Unlike some prior compilations in the literature, we include the date of CPT testing, should analysts wish to consider it.

Second, while the depth of CPT penetration is assumed to be the limiting depth of potentially liquefiable soil, the possibility of premature refusal (i.e., termination on shallow gravels that overlay susceptible materials) is difficult to refute. This possibility was mitigated by making use of the plentiful borings in the affected area, which were used to identify and eliminate provisional case histories with a higher likelihood of premature refusal. One exception, for which some degree of additional uncertainty exists, is case #4 (Harbor Island-01). From several adjacent borings, the CPT at this site is interpreted to have terminated on gravel near a depth of 8 m, which in the adjacent borings is underlain by sandy gravels and gravelly sands of reported medium density. Hence there is some possibility of additional, potentially liquefiable soil, albeit the SPT data indicate that the materials least resistant to liquefaction reside within the extent of the CPT.

Third, an estimate of the *GWT* depth is needed both at the time of in-situ testing and at the time of the earthquake. The former is required for stress-normalization of CPT data (i.e., routine processing), while the latter is used to infer saturation and compute the imposed cyclic stress. In this regard, the Nisqually earthquake impacted a region characterized by relatively wet winters and relatively dry summers, which could give rise to temporally fluctuating *GWT* depths. In the present effort, and like most prior case histories, the *GWT* at the time of the earthquake can only be estimated from measurements at other times. Of the 24 CPTs, 18 were performed during what we interpret to be the wet season, consistent with the Nisqually earthquake's occurrence in February. Analyses of the remaining six, which were performed during what we interpret to be drier months, give no indication of bias (i.e., the computed liquefaction hazards, as subsequently computed and presented herein, do not appear systematically suppressed, which could occur if the *GWT* depths at the time of the earthquake were overestimated). Nonetheless, because one *GWT* depth is used to represent conditions at the times of both testing and shaking, this depth should be viewed as an uncertain quantity.

Fourth, PGA was estimated at study sites by conditioning GMM predictions on groundmotion recordings. Inherent to this approach, and to the fundamental way in which "stress-based" liquefaction models are trained, this PGA should be that which occurs in the absence of liquefaction. Notably, four strong-motion instruments (stations SDS, SDW, HAR, and BOE) – all in the Duwamish River valley immediately south of downtown Seattle - were in areas where liquefaction was observed during the Nisqually earthquake (e.g., Frankel et al., 2002). It is well established that liquefaction can influence ground-motion records, typically in the form of highfrequency acceleration pulses due to the soil's cyclic mobility/dilation response, and a subsequent reduction in high frequency motion due to softening from liquefaction (e.g., Kramer et al., 2016). Each of these effects could influence a recorded PGA (i.e., augment or suppress it), and in turn, influence the conditional PGAs computed at case-history sites, especially if proximal to an affected instrument. Of the four stations above, Zhan and Chen (2021) reported little or no evidence of liquefaction in the records from stations SDS and HAR, which may be attributable to the generally minor liquefaction observed in these areas (i.e., SODO district and Harbor Island), or otherwise indicate that soil directly beneath the instruments did not liquefy. As noted by Zhan and Chen (2021), however, the records from stations BOE and SDW do show possible evidence of liquefaction, especially for the latter. If the PGAs recorded at these stations are associated with a high frequency dilation pulse, this PGA could exceed that which would have occurred in the absence of liquefaction. It has been suggested in such cases (e.g., Upadhyaya et al., 2019) that taking the PGA prior to any inferred evidence of liquefaction may be more appropriate. However, whereas a dilation pulse could artificially increase the PGA, selecting a peak value prior to evidence of liquefaction may artificially reduce it. Thus, the "true" PGA – sans liquefaction – cannot be known with confidence. For this study, station record SDW was removed from the analyses, given its proximity to case histories in Seattle's SODO district and the interpreted strong evidence of liquefaction. Conversely, the record from BOE was retained despite this uncertainty. While case history #9 (Boeing Field-01) shares the namesake of the potentially dubious BOE station, it is located more than 1 km from BOE and much nearer to a station without inferred evidence of liquefaction. Additionally, the recorded PGA at BOE was not a spatial outlier (i.e., not unexpectedly high or low). Thus, while the possibility of unwanted influence persists in the dataset, this influence is judged to be quite minimal, given the large number of recording stations in the

region and fact that very few are believed to have been impacted by liquefaction. Nonetheless, analysts should be aware of this issue.

Fifth, and following from above, conditional PGAs were estimated at study sites using several site and region-specific inputs and components, such as the Goda and Atkinson (2009) spatial correlation model. While this model was developed specifically for subduction zone settings, it may be possible to instead develop and use an event-specific correlation model, given the large number of records, albeit most case histories compiled herein are relatively close to recording stations, so PGA estimates would likely be very similar. Similarly, selecting other GMMs, basin maps, V_{S30} values, etc. would invariably change the PGA estimates at study sites.

Performance Assessment of Liquefaction Response Models

Evaluation Methodology

Six CPT-based liquefaction triggering models will be tested using the newly compiled data. These include Robertson and Wride (1998) [RW98], Architectural Institute of Japan (2001) [AIJ01], Moss et al. (2006) [Mea06], Idriss and Boulanger (2008) [IB08], Boulanger and Idriss (2016) [BI16], and Green et al. (2019) [Gea19]. However, because these models predict the incidence of liquefaction as a function of depth within a profile, whereas the field observations of liquefaction response were made at the ground surface, the triggering models cannot be directly evaluated. This discrepancy is not unique to the Nisqually earthquake, but rather, is characteristic of essentially all existing liquefaction case histories, given the extreme difficulty and expense of determining which strata, at which depths, did or did not liquefy. While past studies have evaluated triggering models by selecting one "critical layer" from the profile, this selection is highly subjective and invites confirmation bias. Different analysts will invariably select different critical strata and different representative properties for those strata, meaning that nearly any a priori assumption of model superiority may be corroborated. Accordingly, to objectively compare predictions to field observations, each of the six triggering models will be used in series with three separate models that predict surficial manifestations of liquefaction: (i) the liquefaction potential index, or LPI, proposed by Iwasaki et al. (1978); (ii) a modified LPI, termed LPI_{ISH}, proposed by Maurer et al. (2015b), and (iii) the liquefaction severity number, or LSN, of van Ballegooy et al. (2014). For brevity, and because LPI, LPIISH, and LSN are well known in the literature, their definitions are omitted here but are exactly as described in Geyin et al. (2020). For consistency with how LPI,

*LPI*_{ISH}, and *LSN* are defined and routinely computed in practice, liquefaction triggering was computed using the deterministic version of each triggering model. Given the six triggering models and three manifestation models, a total of 18 prediction models will be evaluated.

Of course, this approach to model evaluation also calls attention to the paradoxical way in which triggering models have been developed and used. Specifically, and as discussed by Geyin et al. (2020) and Upadhyaya et al. (2022), the development of a triggering model inherently requires use of a manifestation model, given that surficial evidence presents an inverse problem. Liquefaction could conceivably occur in different strata, at different depths, and to differing degrees (or not at all) but produce a manifestation that is perceptibly the same. The developers of triggering models, however, have to-date used manifestation models defined by personal and generally unknown judgements, rather than by analytical expressions (e.g., *LPI*). This makes it impossible to evaluate the triggering models in a manner consistent with their respective developments, given that the manifestation model used to develop a triggering model, and that subsequently used with the model to make forward predictions, are not the same. Our evaluation is thus acknowledged to be less than completely rational but completely consistent with the current state-of-practice.

To make predictions of surface manifestation, and to facilitate comparison with other global case histories, the "global" fragility functions of Geyin and Maurer (2020), which are conditioned on LPI, LPI_{ISH} , and LSN, will be used to compute probabilities of surface manifestation for each of the 24 Nisqually case histories. These functions were previously trained on a large compilation of existing global case histories and are specific to each of the 18 models evaluated herein (i.e., the function coefficients are specific to the adopted triggering and manifestation model). Prior to using any of the six triggering models, liquefaction susceptibility was inferred from the CPT soil behavior type index (I_c) (Robertson and Wride, 1998). However, because the relationship between I_c and susceptibility is uncertain, the I_c – susceptibility model of Maurer et al. (2019) was used to probabilistically predict susceptibility, as defined by Boulanger and Idriss (2006), from the measured I_c . While this model was trained on data from New Zealand, it is the only known model of its type and its applicability elsewhere has not been disproven. Ultimately, our accounting for the uncertain relationship between I_c and susceptibility is generally inconsequential. Nonetheless, to include this uncertainty, as well as that of the estimated PGA for each case history, the probability of manifestation is computed as:

$$P(\text{Manifestation}) = \int_{PGA} \int_{I_c} P(\text{Manifestation}|PGA, I_c \ threshold) \ f(I_c) f(PGA) \cdot dI_c \cdot dPGA \quad (8)$$

Where $f(I_c threshold)$ is the probability density function (PDF) of the I_c threshold for discriminating susceptibility (Maurer et al., 2019); f(PGA) is the PDF of conditional PGA, as computed herein for each case history (e.g., Eq. 7); and $P(Manifestation|PGA, I_c threshold)$ is the probability of surficial manifestation, which is conditioned on PGA and the threshold I_c for determining susceptibility, among numerous other inputs, and which is computed via the fragility functions of Geyin and Maurer (2020):

$$F_{M}(LMM) = \Phi\left(\frac{\ln(LMM) - \ln(\theta)}{\beta}\right) \tag{9}$$

Where $F_M(LMM)$ is the probability of surface manifestation conditioned on a liquefaction manifestation model (LMM) index value; Φ is the Gaussian cumulative distribution function, and θ and β are the distribution's median and logarithmic standard deviation, respectively, and are obtained from Table 4 of Geyin and Maurer (2020) for each of the 18 models.

Model efficiency will be evaluated using receiver operating characteristic (ROC) analyses, which are ubiquitous in science, engineering, medicine, etc. (e.g., Fawcett, 2006) and widely used in earthquake engineering. Specifically, the area under the ROC curve (AUC) will be used to quantify performance. AUC is a particularly attractive measure of efficiency when working with class-imbalanced data, as is common for liquefaction datasets. Whereas measures like overall accuracy are sensitive to this sampling bias and may thus give the impression that biased models are better than unbiased models, AUC is not (Fawcett, 2006). In the context of this study, AUC is the probability that sites with manifestations have higher computed probabilities of manifestation than sites without manifestations. Models with higher AUC are thus more efficient. However, to evaluate whether differences in AUC could happen by chance (i.e., due to the finite sampling of case histories), tests of statistical significance will be performed using the technique of DeLong et al. (1988), which is specific to ROC analyses. Each model will be compared against all others to determine which, if any, is significantly better. Finally, the optimum operating point, or OOP, will be computed from ROC analyses of each model. In the context of this study, the OOP is the computed probability of manifestation that most optimally separates cases with and without observed manifestations. An OOP much less than 50% would suggest that liquefaction manifestations occurred more readily than expected in the Nisqually dataset, as compared to the

Geyin and Maurer (2020) analyses of other global case histories. In other words, this would suggest that the liquefaction hazard is underpredicted in the Nisqually event based on the calibrated median behavior of the model in prior earthquakes. Conversely, an *OOP* greater than 50% would indicate that manifestations occurred less readily than expected and that the hazard is to some degree overpredicted by the Geyin and Maurer (2020) fragility functions. Similar to the interpretation of *AUC*, confidence intervals will be computed for each model's *OOP* using bootstrap sampling, thereby accounting for the finite-sample uncertainty of *OOP* values. From these confidence intervals, it can be determined whether any deviations of the *OOP*s from 50% are statistically significant.

Model Evaluation Results and Discussion

Using the data and methodology above, 18 models were used to predict probabilities of surface manifestation for 24 case histories. These predicted probabilities are presented in Table 3, where the prediction averaged across the 18 models is also shown for each case history. Considering all cases, sites with observed manifestations have average probabilities ranging from 0.12 to 0.79 whereas sites without observed manifestations have average probabilities ranging from 0.00 to 0.40. It may be observed that the predictions made by the 18 models often vary considerably for a given case history. The difference between the highest and lowest predicted probability, for example, exceeds 0.50 for 6 cases and exceeds 0.30 for 12 cases. These large differences indicate that the cases may be useful for resolving discrepancies amongst the models (i.e., that the soil is near the modeled threshold for triggering over several meters of the subsurface). To facilitate case-history selection and interpretation for various uses, profiles of the cone-tip resistance normalized for overburden and corrected for fines content (q_{clnes}), cyclic stress ratio (CSR), I_c , and factor of safety against liquefaction triggering (FoS) are provided in the appendix for each case history. These figures utilize the Boulanger and Idriss (2016) model to compute q_{clnes} , CSR, and FoS and an example is shown in Figure 4 for case-history no. 12.

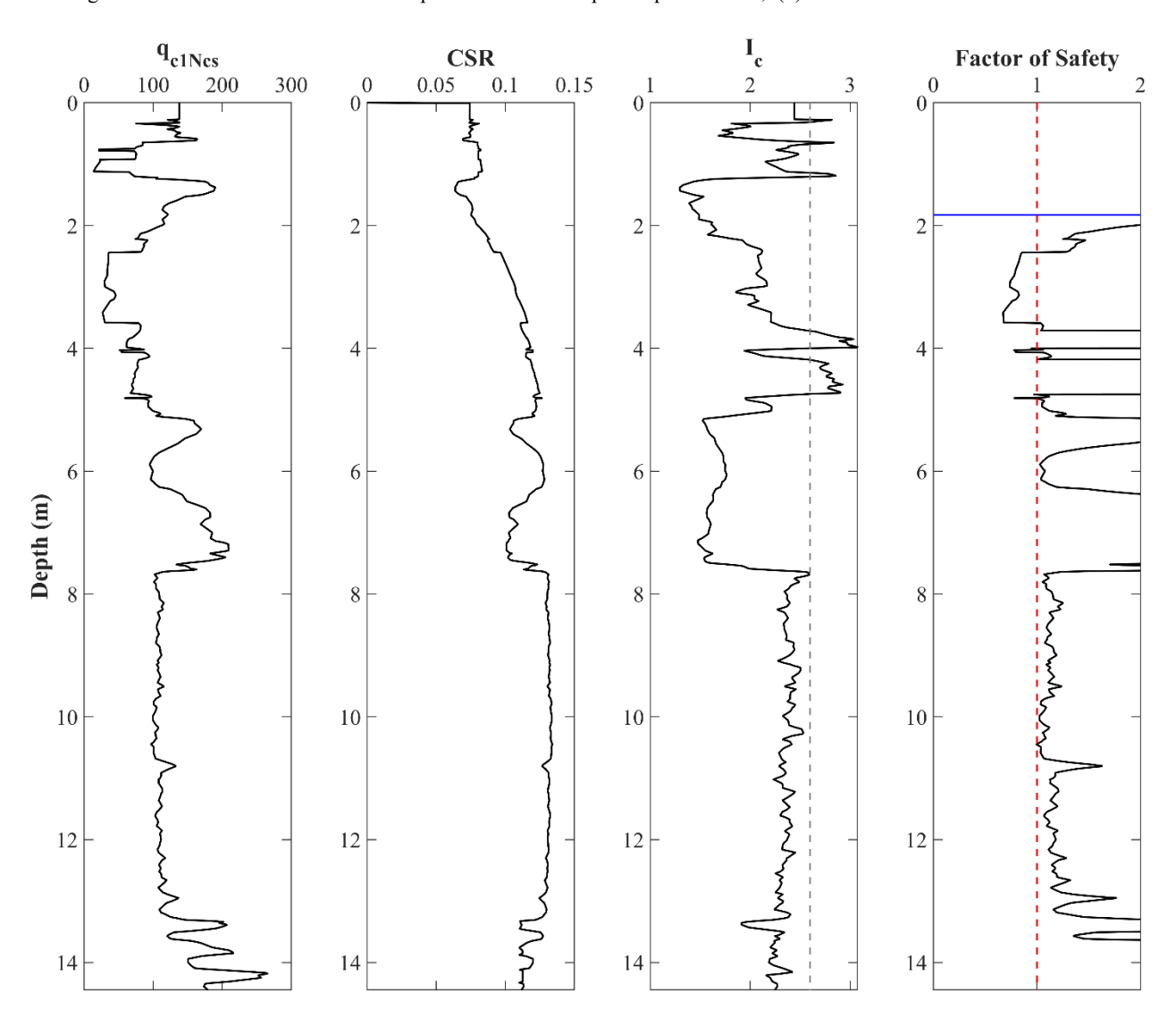


Figure 4. Computed q_{cIncs} , CSR, I_c , and FoS for case history no. 12 (Elliot Ave-01), as described in the text; analogous figures are provided in the appendix for all 24 case histories.

Several observations can be made from the plots like that in Figure 4. First, and as suggested by the large variance across model predictions, many profiles contain soils very near the expected threshold for liquefaction. The case history in Figure 4 is one such example, in that \sim 6 m of the profile has computed FoS between 0.8 and 1.2. Second, all "no manifestation" case-history sites are inferred to contain deposits susceptible to liquefaction (e.g., soils with $I_c < 2.6$) that would be expected to trigger under sufficient seismic loading; these inferences were also confirmed by proximal borings in each case. Third, it can also be seen that many "no manifestation" cases contain deposits expected to liquefy by one or more triggering model. The case in Figure 4 is one

of several examples where triggering is predicted but no manifestation is observed. These cases may help to resolve discrepant predictions amongst triggering models and/or further elucidate the complex relationship between the triggering and surficial manifestation of liquefaction.

To quantify model efficiency, ROC analyses were performed and are summarized in terms of AUC in Table 4; additionally, ROC plots are provided in the appendix for each of the 18 models. The top-performing models include BI16-LPI (i.e., the BI16 triggering model used with the LPI manifestation model) and RW98-LPI, which each have an AUC of 0.926. For context, an AUC of 0.5 corresponds to random guessing (i.e., there is a 50% probability that sites with manifestations have higher model predictions than sites without manifestations). In the case of a perfectly efficient model, this probability is 100% (i.e., AUC is 1). Nearly as efficient as these models are BI16-LPI_{ISH} and Gea-LPI (AUC = 0.919). The least efficient model for this dataset is Mea06-LSN (AUC = 0.793), albeit its performance is still nearer to a perfect model than to random guessing. Notably, the computed AUC values have relatively large finite-sample uncertainties, given the limited number of compiled case histories. If these 24 cases were hypothetically selected from a much larger population of case histories, then different samples of 24 cases would likely result in different AUC values, and in turn, different assessments of model superiority. In this way, AUC values are more uncertain when based on a small sample of the population, all else being equal, and there is less confidence that any one sample (e.g., an observed difference in model performance) accurately reflects the overall population. This uncertainty also increases further as the sample becomes more heterogeneous, indicating that a larger sample is required to accurately represent the population at large.

Table 3. Probabilities of surficial liquefaction manifestations (i.e., "ground failure"), as predicted by 18 models for 24 case histories.

Case	Surface		RW98		AIJ01		Mea06			IB08			BI16			Gea19				
History No.	Manifestation	LPI	LPI_{ISH}	LSN	LPI	LPI_{ISH}	LSN	LPI	LPI_{ISH}	LSN	LPI	LPI_{ISH}	LSN	LPI	LPI_{ISH}	LSN	LPI	LPI_{ISH}	LSN	Average
1	Yes	0.75	0.82	0.90	0.68	0.74	0.65	0.80	0.86	0.88	0.73	0.79	0.89	0.73	0.78	0.89	0.74	0.77	0.90	0.79
2	Yes	0.35	0.31	0.46	0.42	0.34	0.31	0.37	0.35	0.46	0.34	0.32	0.45	0.46	0.45	0.50	0.45	0.46	0.50	0.41
3	Yes	0.08	0.14	0.12	0.05	0.07	0.06	0.14	0.19	0.20	0.13	0.19	0.18	0.13	0.22	0.18	0.14	0.29	0.19	0.15
4	Yes	0.06	0.08	0.19	0.04	0.04	0.11	0.05	0.09	0.18	0.08	0.20	0.18	0.05	0.17	0.18	0.06	0.25	0.18	0.12
5	Yes	0.34	0.22	0.68	0.52	0.36	0.65	0.38	0.30	0.77	0.30	0.29	0.65	0.43	0.35	0.76	0.44	0.39	0.75	0.48
6	Yes	0.11	0.03	0.32	0.25	0.09	0.33	0.42	0.31	0.62	0.12	0.06	0.32	0.22	0.08	0.43	0.22	0.08	0.45	0.25
7	Yes	0.09	0.03	0.23	0.03	0.01	0.10	0.41	0.34	0.59	0.17	0.10	0.30	0.15	0.07	0.28	0.15	0.07	0.29	0.19
8	Yes	0.50	0.34	0.63	0.59	0.51	0.51	0.61	0.56	0.69	0.38	0.32	0.58	0.57	0.53	0.74	0.60	0.59	0.76	0.56
9	Yes	0.25	0.22	0.45	0.28	0.22	0.41	0.44	0.45	0.60	0.28	0.27	0.43	0.32	0.31	0.51	0.32	0.35	0.53	0.37
10	No	0.05	0.02	0.15	0.04	0.01	0.11	0.21	0.20	0.38	0.11	0.08	0.23	0.12	0.07	0.25	0.11	0.06	0.25	0.14
11	No	0.00	0.00	0.00	0.00	0.00	0.00	0.00	0.00	0.02	0.00	0.00	0.00	0.00	0.00	0.00	0.00	0.00	0.00	0.00
12	No	0.16	0.16	0.64	0.17	0.18	0.44	0.37	0.40	0.73	0.28	0.39	0.71	0.21	0.30	0.70	0.25	0.42	0.72	0.40
13	No	0.05	0.03	0.24	0.04	0.00	0.18	0.17	0.14	0.47	0.08	0.08	0.27	0.04	0.05	0.25	0.04	0.11	0.27	0.14
14	No	0.00	0.00	0.00	0.00	0.00	0.01	0.00	0.00	0.05	0.00	0.00	0.01	0.00	0.00	0.01	0.00	0.00	0.01	0.00
15	No	0.07	0.11	0.17	0.05	0.05	0.07	0.17	0.29	0.44	0.08	0.15	0.18	0.10	0.17	0.19	0.11	0.22	0.23	0.16
16	No	0.00	0.00	0.00	0.00	0.00	0.00	0.00	0.00	0.03	0.00	0.00	0.01	0.00	0.00	0.00	0.00	0.00	0.01	0.00
17	No	0.00	0.00	0.00	0.00	0.00	0.00	0.00	0.00	0.02	0.00	0.00	0.00	0.00	0.00	0.00	0.00	0.00	0.00	0.00
18	No	0.08	0.04	0.20	0.05	0.01	0.08	0.29	0.33	0.55	0.14	0.12	0.28	0.10	0.06	0.23	0.11	0.11	0.27	0.17
19	No	0.05	0.12	0.17	0.01	0.03	0.07	0.19	0.22	0.40	0.11	0.22	0.27	0.07	0.19	0.24	0.08	0.30	0.26	0.17
20	No	0.01	0.00	0.02	0.00	0.00	0.00	0.08	0.05	0.25	0.03	0.01	0.08	0.01	0.00	0.04	0.01	0.00	0.05	0.04
21	No	0.00	0.00	0.03	0.00	0.00	0.01	0.07	0.07	0.24	0.02	0.01	0.08	0.01	0.00	0.04	0.01	0.00	0.05	0.04
22	No	0.16	0.10	0.43	0.20	0.13	0.35	0.29	0.22	0.61	0.20	0.18	0.48	0.18	0.16	0.46	0.19	0.21	0.50	0.28
23	No	0.00	0.00	0.00	0.00	0.00	0.00	0.01	0.00	0.04	0.00	0.00	0.01	0.00	0.00	0.00	0.00	0.00	0.00	0.00
24	No	0.01	0.00	0.02	0.01	0.00	0.01	0.04	0.01	0.11	0.03	0.01	0.05	0.03	0.01	0.04	0.02	0.00	0.04	0.02

Table 4. Summary of liquefaction model performance, as quantified by *AUC* (the area under a receiver operating characteristic (ROC) curve).

Model	RW98	AIJ01	Mea06	IB08	BI16	Gea19
LPI	0.926	0.896	0.874	0.889	0.926	0.919
LPIISH	0.881	0.911	0.859	0.852	0.919	0.867
LSN	0.859	0.859	0.793	0.830	0.852	0.852

Accordingly, to evaluate whether the differences in AUC reported in Table 4 are statistically significant, p-values were computed per DeLong et al. (1988) to compare each model's AUC to all others. These values are given in Table 5 and are the probabilities that AUC values from two models came from the same distribution. That is, the probability that an observed difference in model performance is due to finite sampling (as opposed to real differences in performance). We adopt the significance level of 0.1, such that p-values below this are deemed statistically significant (i.e., there is at least 90% confidence the models are different). Smaller pvalues are generally expected when: (i) the dataset is large and relatively homogeneous; and (ii) the prediction models have large observed differences in performance, which is to say the predictions are not strongly correlated. Based on this threshold, Table 5 compares all model pairs and indicates whether either model is better – to a statistically significant degree – via the cell shading. If the cell is shaded grey, the model in the top row is better, whereas if the cell is shaded orange, the model in the left column is better. If the cell is unshaded, the models are not significantly different. The most salient findings from Table 5 are as follows. First, no model is significantly better than all others. Second, most of the measured differences in model performance (i.e., Table 4) are not statistically significant. Of the 153 model comparisons made in Table 5, just 13 are significant. While this number would increase if the 0.1 threshold were relaxed (e.g., to 29 using the unusual threshold of 0.2), the overall conclusion is that little can be confidently said about model superiority. Third, the models with significantly different performance are largely models based on LSN, which when compared to the best-performing models (e.g., BI16-LPI), are significantly less efficient.

Rasanen RA, Geyin M, Maurer BW. Select liquefaction case histories from the 2001 Nisqually, Washington, earthquake: A digital data set and assessment of model performance. Earthquake Spectra. 2023;0(0). doi:10.1177/87552930231174244

Table 5. Summary of p-values computed to compare the performance of each model, as quantified via AUC, to all others.

p-va		LPI							LPI _{ISH}							LSN					
matrix ¹		RW98	AIJ01	Mea06	IB08	BI16	Gea19	RW98	AIJ01	Mea06	IB08	BI16	Gea19	RW98	AIJ01	Mea06	IB08	BI16	Gea19		
	RW98		0.509	0.432	0.122	1.000	0.734	0.339	0.573	0.193	0.234	0.856	0.311	0.151	0.174	0.054	0.044	0.114	0.114		
	AIJ01			0.746	0.880	0.409	0.564	0.802	0.705	0.558	0.582	0.709	0.673	0.545	0.539	0.174	0.310	0.446	0.446		
IHI	Mea06				0.802	0.302	0.400	0.935	0.642	0.724	0.833	0.616	0.942	0.814	0.833	0.056	0.448	0.577	0.577		
T	IB08					0.227	0.207	0.880	0.580	0.448	0.557	0.562	0.718	0.521	0.580	0.117	0.138	0.328	0.328		
	BI16						0.480	0.446	0.707	0.150	0.338	0.889	0.409	0.223	0.252	0.036	0.054	0.094	0.094		
	Gea19							0.483	0.840	0.168	0.338	1.000	0.432	0.244	0.286	0.045	0.050	0.104	0.104		
	RW98								0.430	0.757	0.462	0.161	0.625	0.751	0.754	0.355	0.496	0.675	0.675		
	AIJ01									0.418	0.283	0.810	0.337	0.322	0.300	0.142	0.178	0.305	0.305		
LPI _{ISH}	Mea06										0.924	0.404	0.924	1.000	1.000	0.184	0.491	0.810	0.810		
LP	IB08											0.075	0.530	0.914	0.917	0.562	0.774	1.000	1.000		
	BI16												0.087	0.358	0.351	0.180	0.224	0.333	0.333		
	Gea19													0.912	0.913	0.466	0.641	0.846	0.846		
	RW98														1.000	0.176	0.385	0.811	0.811		
	AIJ01															0.235	0.482	0.852	0.852		
NST	Mea06																0.364	0.094	0.094		
77	IB08																	0.414	0.414		
	BI16																		1.000		
	Gea19																				

¹Cell values are the probabilities that *AUC* samples for two models could have come from the same distribution. Values less than 0.1 are deemed "significant," in which case the model with significantly better performance is indicated via the cell shading.

Each of these findings is generally consistent with analogous analyses previously performed for global CPT-based case histories (Geyin et al., 2020). This calls attention to the general inappropriateness of championing prediction models based on observations in individual earthquakes, and to the ongoing needs for additional case-history data and more rigorous adherence to best practices in model training and testing. With few exceptions (e.g., the Canterbury earthquake sequence of the 2010's), case histories compiled from individual earthquakes – or even from many earthquakes – are insufficient to establish statistically significant differences in model performance. Yet numerous papers have trained, calibrated, or tested liquefaction response models using small datasets, with many deriving claims of model superiority. Tests of statistical significance are exceedingly rare in the liquefaction literature, however, and if presented, would likely change the perception of prominent works. Additionally, published models are in many instances never tested against existing models. None of the six liquefaction triggering models evaluated herein, for example, was tested against any other model when originally proposed. The same is true for many models that predict manifestations of liquefaction. While such practices would be objectionable in many fields, they have passed as acceptable in geotechnical engineering.

Finally, the OOP, or computed probability of manifestation that most optimally separates cases with and without observed manifestations, was extracted from the ROC analyses. An OOP of 0.19 was computed for the probability of manifestation averaged across all 18 models, suggesting that liquefaction manifestations may have occurred more readily than expected by the Geyin and Maurer (2020) fragility functions. That is, the liquefaction hazard may have been underpredicted based on calibrations of the 18 models against global case histories. If so, this apparent bias could have several causes. First, the observed manifestations of liquefaction were largely "minor" except for cases #9 (Boeing Field-01) and #1 (Capital Lake-01), where manifestations could be classified as more severe per the criteria of Maurer et al. (2014a). If the criteria for selecting "positive" case histories were historically more stringent (i.e., requiring more severe manifestations to draw attention and warrant documentation), this might impart a tendency in the Geyin and Maurer (2020) fragility functions to underpredict minor manifestations, being that the functions are based on global and generally older case histories. This is plausible, given that relatively less severe liquefaction might be overlooked if not in a major city such as Seattle. As an example, case #6 (SODO-02) lacked ejecta but was interpreted to be a site of liquefaction based on cracking and differential settlements observed in payement. In this case and others, where the observed manifestations were relatively minor, it might be expected that the computed liquefaction hazards would be on the lower end of the spectrum for "positive" sites. It has similarly been observed that lateral spreading may occur at low *LSN*, *LPI*, and *LPI*_{ISH} values (e.g., Maurer et al., 2015c), given that it can result from a thin liquefied stratum that would not otherwise produce ejecta or large settlements. Case #3 (Capitol Lake-02), which had a low computed probability of manifestation, involved a possible spreading crack and a trace amount of ejecta. In the absence of the crack, however, it might be conjectured that liquefaction would not have manifested.

Second, 17 of the 24 case histories map to artificial fill. While this is not unusual in the context of global case histories, it nonetheless may explain the greater-than-expected liquefaction response, which could be expected to increase with decreasing deposit age, all else being equal. CPT penetration resistance does fully capture small-strain soil aging effects (e.g., Maurer et al., 2014b) and correction factors to account for this shortcoming in young deposits (e.g., Bwambale and Andrus, 2019) were not used. Third, many of the case histories were compiled from the Seattle basin (as evidenced by large $Z_{1.0}$ and $Z_{2.5}$ values – see Table S1), which could result in more cycles of seismic loading than expected. While liquefaction models account for the influence of nearsurface conditions on cyclic demand at depth, no model explicitly considers the effects of deep sediment basins. As such, liquefaction might occur more readily where strong basin effects are observed, given that these effects can increase the duration of loading. Similarly, there are relatively few subduction zone events in the datasets used to train existing liquefaction models and model components, which may result in predictions with more uncertainty, or even bias, in subduction zone settings. This is particularly the case for large-magnitude interface ruptures, such as that which occurred in the Cascadia Subduction Zone 323 YBP and many times prior. In this regard, further research is needed to assess or improve the applicability of state-of-practice liquefaction models to subduction zone settings, which might entail the development of regionspecific models (e.g., Green et al., 2020). Of course, we must add to the above various other possible causes for the apparent underprediction of liquefaction response, including other fundamental shortcomings in the models used to predict liquefaction triggering and/or its surficial manifestation.

However, like *AUC* values the finite-sample uncertainty of *OOP*s should be considered, given the limited number of case histories. To account for this uncertainty, bootstrap sampling of the 24 cases was used to compute a 95% confidence interval for the *OOP* averaged across all

models. This interval ranged from 0.12 to 0.56, and as such, it cannot be confidently concluded that the *OOP* is less than 0.5 (i.e., that the Nisqually case histories deviate from median global behavior). Thus, while liquefaction manifestations may have occurred more readily than expected for the Nisqually dataset, additional case histories would be needed to confirm this, or to draw any definitive conclusion about performance and bias. The large uncertainty of the *OOP* again alludes to the dangers of training or calibrating a liquefaction model with limited data (e.g., from a single earthquake), as researchers have opted for, or been resigned to, throughout the existing literature.

Conclusions

While liquefaction is observed in nearly all moderate to large earthquakes, the data needed to train state-of-practice liquefaction prediction models has remained relatively scarce, owing to its cost and variety. This lack of data inhibits the training and testing of better models. Accordingly, this paper compiled and preliminarily analyzed 24 CPT-based case histories from the 2001 Nisqually, Washington, earthquake, which affected the Puget Sound of the U.S. Pacific Northwest. The cases were compiled from the free field on ground that is generally level, are among very few in the literature associated with subduction zone earthquakes, and collectively represent one of the largest compilations from a U.S. earthquake to date. Subsequent analyses of the data using 18 different prediction models revealed differences in model efficiency, albeit these differences were rarely statistically significant when considering finite-sample uncertainty. While these measurements used a particular metric of efficiency (AUC), it is our judgement that this overall result would stand independent of the metric chosen. This conclusion alludes to the general inappropriateness of championing models based on individual earthquakes or otherwise small datasets, as is frequently done in the literature without statistical backing. This also calls attention to the obvious and ongoing need for more data. The Nisqually case histories provide a useful addition for model training and testing but must be combined with existing case histories (e.g., Brandenberg et al., 2020; Montalva et al., 2021; Geyin et al., 2021) and others not yet collected.

Data Availability

The compiled dataset is available in digital format through both the DesignSafe Data Depot at https://doi.org/10.17603/ds2-nsf8-7944 and in an electronic appendix to this paper, where supplemental figures are also provided.

Funding

The presented study is based on work supported by the National Science Foundation (NSF) under Grant No. CMMI-1751216 and by the NSF Graduate Research Fellowship Program under Grant No. DGE-1762114. However, any opinions, findings, and conclusions or recommendations expressed in this paper are those of the authors and do not necessarily reflect the views of NSF.

Acknowledgements

The authors gratefully acknowledge the many individuals who contributed to post-earthquake reconnaissance following the Nisqually earthquake as well as Silvia Mazzoni of the John Garrick Institute for Risk Sciences at UCLA for coding the ground motion model utilized in this study.

References

- AGRA Earth & Environmental, Inc. (1996) Subsurface Exploration and Preliminary Geotechnical Engineering Report ICA Soccer and Baseball Field Development Seattle, Washington. May 28, 1996. Available from Washington State Department of Natural Resources Washington Geologic Information Portal, last accessed May 10, 2022.
- Ahdi S.K., Ancheta T.D., Contreras V., Kishida T., Kwak D.Y., Kwok O.L., Parker G.A., Stewart J.P. 2020. *Chapter 5: Site Condition Parameters*. PEER Report No. 2020/03, J.P. Stewart (ed.), Pacific Earthquake Engineering Research Center, University of California, Berkeley, CA.
- Bassal, PC, and Boulanger, RW. 2021. System response of an interlayered deposit with spatially preferential liquefaction manifestations. *Journal of Geotechnical and Geoenvironmental Engineering*, 147(12): 05021013.
- Boulanger RW and Idriss IM (2006) Liquefaction susceptibility criteria for silts and clays. *Journal of Geotechnical and Geoenvironmental Engineering* 132(11): 1413-1426.
- Boulanger RW and Idriss IM (2016) CPT-based liquefaction triggering procedure. *Journal of Geotechnical and Geoenvironmental Engineering*, 142(2): 04015065-04015065.
- Boulanger RW and Ziotopoulou K (2015) PM4Sand (Version 3): A sand plasticity model for earthquake engineering applications. Center for Geotechnical Modeling Report No. UCD/CGM-15/01, Department of Civil and Environmental Engineering, University of California, Davis, Calif.
- Bradley BA (2014) Site-specific and spatially-distributed ground motion intensity estimation in the 2010-2011 Christchurch earthquakes. *Soil Dynamics and Earthquake Engineering* 48: 35-47.

- Brandenberg SJ, Zimmaro P, Stewart JP, Kwak DY, Franke KW, Moss RE, ... and Kramer SL (2020) Next-generation liquefaction database. *Earthquake Spectra*, *36*(2): 939-959.
- Bray JD, Sancio R, Kammerer AM, Merry S, Rodriguez-Marek A, Khazai B, ... and Nykamp M (2001) Some observations of the geotechnical aspects of the February 28, 2001, Nisqually earthquake in Olympia, South Seattle, and Tacoma, Washington. Report sponsored by NSF, PEER, UCB, University of Arizona, Washington State University, Shannon and Wilson Inc., and Leighton and Associates.
- Buck JR, Daniel MM and Singer AC (2002) Computer Explorations in Signals and Systems Using MATLAB. 2nd ed. Upper Saddle River, NJ: Prentice Hall.
- Bustin A, Hyndman RD, Lambert A, Ristau J, He J, Dragert H, and Van der Kooij M (2004) Fault parameters of the Nisqually earthquake determined from moment tensor solutions and the surface deformation from GPS and InSAR. *Bulletin of the Seismological Society of America*, 94(2): 363-376.
- Bwambale B and Andrus RD (2019) State of the art in the assessment of aging effects on soil liquefaction. *Soil Dynamics and Earthquake Engineering*, 125: 105658.
- Chleborad AF and Schuster RL (1990) Ground failure associated with the Puget Sound region earthquakes of April 13, 1949 and April 29, 1965. United States Geological Survey Open-File Rept.
- CH2M Hill Engineering Inc. (1989) West Point Treatment Plant Secondary Treatment Facilities ST 08 Liquids Stream: Supplemental Plant Site Geotechnical Data Report. April 1989. Available from Washington State Department of Natural Resources Washington Geologic Information Portal, last accessed May 10, 2022.
- Dames and Moore (1997) Report of Geotechnical Investigation King Street Yard Maintenance Facility Seattle, Washington. November 12, 1997. Available from Washington State Department of Natural Resources Washington Geologic Information Portal, last accessed May 14, 2022.
- DeLong ER, DeLong DM and Clarke-Pearson DL (1988) Comparing the areas under two or more correlated receiver operating characteristic curves: a nonparametric approach. *Biometrics* 44: 837-845.
- de Magistris, FS, Lanzano, G, Forte, G, and Fabbrocino, G (2013) A database for PGA threshold in liquefaction occurrence. *Soil Dynamics and Earthquake Engineering* 54: 17-19.
- Earth Consultants Inc. (1992) Geotechnical Engineering Study Home Depot SODO Center 1st Avenue South and South Forest Street, Seattle, Washington. October 23, 1991. Available from Washington State Department of Natural Resources Washington Geologic Information Portal, last accessed May 14, 2022.
- Fawcett T (2006) An introduction to ROC analysis. Pattern Recognition Letters 27(8): 861-874.
- Frankel AD, Carver DL, & Williams RA (2002) Nonlinear and linear site response and basin effects in Seattle for the M 6.8 Nisqually, Washington, earthquake. *Bulletin of the Seismological Society of America*, 92(6): 2090-2109.
- GeoEngineers, Inc. (1990) Geotechnical Report 1135 S. Webster Street, Seattle, Washington. September 11, 1990. Available from Washington State Department of Natural Resources Washington Geologic Information Portal, last accessed May 10, 2022.
- GeoEngineers, Inc. (1993) Geotechnical Engineering Services Proposed Thoroughbred Racing Facility Auburn, Washington. June 16, 1993. Available from Washington State Department of Natural Resources Washington Geologic Information Portal, last accessed May 12, 2022.
- GeoEngineers, Inc. (2003) Summary Geotechnical Report Ground Improvement and Foundation Support Old Seattle Chocolate Factory Site, Seattle, Washington. July 22, 2003. Available from Washington State Department of Natural Resources Washington Geologic Information Portal, last accessed May 17, 2022.
- Geyin M and Maurer BW (2020) Fragility functions for liquefaction induced ground failure. *Journal of Geotechnical and Geoenvironmental Engineering*, 146(12): 04020142.

- Geyin M, Baird AJ, and Maurer BW (2020) Field assessment of liquefaction prediction models based on geotechnical vs. geospatial data, with lessons for each. *Earthquake Spectra* 36(3): 1386–1411.
- Geyin M and Maurer BW (2021) Evaluation of a cone penetration test thin-layer correction procedure in the context of global liquefaction model performance. *Engineering Geology*, 291, 106221.
- Geyin M, Maurer BW, and Christofferson K (2022) An AI driven, mechanistically grounded geospatial liquefaction model for rapid response and scenario planning. *Soil Dynamics and Earthquake Engineering*, 159, 107348.
- Geyin M, Maurer BW, Bradley BA, Green RA, and van Ballegooy S (2021). CPT-based liquefaction case histories compiled from three earthquakes in Canterbury, New Zealand. *Earthquake Spectra*, 37(4), 2920-2945.
- Goda K and Atkinson GM (2009) Probabilistic Characterization of Spatially Correlated Response Spectra for Earthquakes in Japan. *Bulletin of the Seismological Society of America* 99(5): 3003-3020.
- Green RA, Bommer JJ, Rodriguez-Marek A, Maurer BW, Stafford PJ, Edwards B, Kruiver PP, De Lange G and Van Elk J (2019) Addressing limitations in existing 'simplified' liquefaction triggering evaluation procedures: application to induced seismicity in the Groningen gas field. *Bulletin of Earthquake Engineering* 17(8): 4539-4557.
- Green RA, Bommer JJ, Stafford PJ, Maurer BW, Kruiver PP, Edwards B, ... & van Elk J (2020) Liquefaction hazard in the Groningen region of the Netherlands due to induced seismicity. Journal of Geotechnical and Geoenvironmental Engineering, 146(8): 04020068.
- Hart-Crowser & Associates, Inc. (1978) Subsurface Exploration Report South 266th Street and South Central Avenue, Kent, Washington. November 1978. Available from Washington State Department of Natural Resources Washington Geologic Information Portal, last accessed May 14, 2022.
- Hart-Crowser & Associates, Inc. (1981) Field Exploration and Geotechnical Engineering Study Proposed J.A. Jones Graving Dock Alexander Avenue and South Lincoln Avenue on Blair Waterway Port of Tacoma, Washington. March 26, 1981. Available from Washington State Department of Natural Resources Washington Geologic Information Portal, last accessed May 14, 2022.
- Hart-Crowser & Associates Inc. (1985) Subsurface Explorations and Geotechnical Engineering Study Proposed Additions to Factoria Square Shopping Center Bellevue, Washington. December 24, 1985. Available from Washington State Department of Natural Resources Washington Geologic Information Portal, last accessed May 10, 2022.
- Hausler EA and Koelling M (2004) Performance of Improved Ground During the 2001 Nisqually Earthquake. *International Conference on Case Histories in Geotechnical Engineering*, New York, New York 18. https://scholarsmine.mst.edu/icchge/5icchge/session03/18
- Ichinose GA, Thio HK, and Somerville PG (2004) Rupture process and near-source shaking of the 1965 Seattle-Tacoma and 2001 Nisqually, intraslab earthquakes. *Geophysical Research Letters*, *31*(10).
- Iwasaki T, Tatsuoka F, Tokida K, and Yasuda SA (1978) Practical method for assessing soil liquefaction potential based on case studies at various sites in Japan. 2nd Int. Conf. on Microzonation, San Francisco.
- Jeschke DA, Eungard DW, Troost KG, Wisher AP (2019) Subsurface Database of Washington State GIS data. Washington Geological Survey Digital Data Series 11, version 2.1, previously released Aug 2017 http://www.dnr.wa.gov/publications/ger portal subsurface database.zip.
- Kao H, Wang K, Chen RY, Wada I, He J, and Malone SD (2008) Identifying the rupture plane of the 2001 Nisqually, Washington, earthquake. *Bulletin of the Seismological Society of America*, 98(3): 1546-1558.

- Kramer SL, Sideras SS and Greenfield MW (2016) The timing of liquefaction and its utility in liquefaction hazard evaluation. *Soil Dynamics and Earthquake Engineering* 91: 133-146.
- Kuehn N, Bozorgnia Y, Campbell KW, and Gregor N (2020) *Partially non-ergodic ground-motion model* for subduction regions using NGA-subduction database. Peer Report 2020/04, Pacific Earthquake Engineering Research Center, University of California, Berkeley, CA.
- Maurer BW, Green RA, Cubrinovski M and Bradley BA (2014a) Evaluation of the liquefaction potential index for assessing liquefaction hazard in Christchurch, New Zealand. *Journal of Geotechnical and Geoenvironmental Engineering* 140(7): 04014032.
- Maurer BW, Green RA, Cubrinovski M, and Bradley BA (2014b) Assessment of aging correction factors for liquefaction resistance at sites of recurrent liquefaction. In 10th national conference proceedings on earthquake engineering. Earthquake Engineering Research Institute, Anchorage, AK.
- Maurer BW, Green RA, Cubrinovski M and Bradley BA (2015a) Calibrating the liquefaction severity number (LSN) for varying misprediction economies: a case study in Christchurch, New Zealand. 6th International Conference on Earthquake Geotechnical Engineering, Paper No. 491.
- Maurer BW, Green RA and Taylor ODS (2015b) Moving towards an improved index for assessing liquefaction hazard: lessons from historical data. *Soils and Foundations* 55(4): 778-787.
- Maurer BW, Green RA, Cubrinovski M, & Bradley BA (2015c) Assessment of CPT-based methods for liquefaction evaluation in a liquefaction potential index framework. *Géotechnique* 65(5): 328-336.
- Maurer BW, Green RA, van Ballegooy S and Wotherspoon L (2019) Development of region-specific soil behavior type index correlations for evaluating liquefaction hazard in Christchurch, New Zealand. *Soil Dynamics and Earthquake Engineering* 117: 96-105.
- McPhillips DF, Herrick JA, Ahdi S, Yong AK, and Haefner S (2020) Updated Compilation of VS30 Data for the United States. *United States Geological Survey* data release, https://doi.org/10.5066/P9H5QEAC.
- Milbor-Pita, Inc. (1996) *Geotechnical Report, Heritage Park, Olympia, Washington*. January 13, 1996. Available from Washington State Department of Natural Resources Washington Geologic Information Portal, last accessed May 14, 2022.
- Moss RES, Seed RB, Kayen RE, Stewart JP, Der Kiureghian A and Cetin KO (2006) CPT-based probabilistic and deterministic assessment of in situ seismic soil liquefaction potential. *Journal of Geotechnical and Geoenvironmental Engineering* 132(8): 1032-1051.
- National Academies of Sciences, Engineering, and Medicine (2016) State of the art and practice in the assessment of earthquake-induced soil liquefaction and its consequences. The National Academies Press. https://doi.org/10.17226/23474.
- Pacific Northwest Seismic Network (2001) Preliminary observations of ground deformation, Nisqually earthquake. Available at: https://assets.pnsn.org/notable/WEBDIR_01022818543p/maps/gd.jpg (Accessed Jan. 31, 2022).
- PacRim Geotechnical, Inc. (1999) Geotechnical Report Pier 17 Renovation Port of Seattle, Washington. July 29, 1999. Available from Washington State Department of Natural Resources Washington Geologic Information Portal, last accessed June 1, 2022.
- Palmer SP, Magsino SL. Bilderback EL, Poelstra JL, Folger DS, Niggemann RA (2007) *Liquefaction* susceptibility and site class maps of Washington State, by county. Open File Report 2004-20, Washington Division of Geology and Earth Resources.
- Parker GA, Stewart JP, Boore DM, Atkinson GM, and Hassani B (2020) NGA-Subduction Global Ground-Motion Models with Regional Adjustment Factors. PEER Report 2020/03, Pacific Earthquake Engineering Research Center, University of California, Berkeley, CA.

- Pinheiro J, Bates DM, DebRoy S, Sarkar D and the R Core Team (2008) NLME: Linear and nonlinear mixed effects models, R Core package, Ver. 3.1, http://www.r-project.org (accessed Mar. 26, 2014).
- Rasanen R, Geyin M, Maurer B (2022) Select CPT-Based Liquefaction Case Histories from the 2001 Nisqually, Washington, Earthquake. DesignSafe-CI. https://doi.org/10.17603/ds2-nsf8-7944 v1.
- Rasanen RA, Marafi NA, and Maurer BW (2021) Compilation and forecasting of paleoliquefaction evidence for the strength of ground motions in the US Pacific Northwest. *Engineering Geology 292*: 106253.
- Rashidian V, and Baise LG (2020) Regional efficacy of a global geospatial liquefaction model. *Engineering geology*, 272: 105644.
- Rateria G and Maurer BW (2022) Evaluation and updating of Ishihara's (1985) model for liquefaction surface expression, with insights from machine and deep learning. *Soils and Foundations* 62(3): 101131.
- Rittenhouse-Zeman & Associates (1987) Subsurface Exploration and Geotechnical Engineering Report Leiendecker Building, Seattle, Washington. August 11, 1987. Available from Washington State Department of Natural Resources Washington Geologic Information Portal, last accessed May 9, 2022.
- Robertson PK and Wride CE (1998) Evaluating cyclic liquefaction potential using cone penetration test. *Canadian Geotechnical Journal* 35(3): 442-459.
- RZA AGRA, Inc. (1993) Subsurface Exploration and Geotechnical Engineering Report Proposed Costco Warehouse Facility Issaquah, Washington. March 10, 1993. Available from Washington State Department of Natural Resources Washington Geologic Information Portal, last accessed May 10, 2022.
- Seattle Office of Emergency Management (2019) Seattle Hazard Identification and Vulnerability Analysis (SHIVA). April 10, 2019. Available from: https://www.seattle.gov/emergency-management/hazards, last accessed May 10, 2022.
- Seed HB and Idriss IM (1971) Simplified procedure for evaluating soil liquefaction potential. *Journal of the Soil Mechanics and Foundations division*, 97(9): 1249-1273.
- Shannon & Wilson, Inc. (1997) Final Geotechnical Data Report Mercer Street Tunnel Contract Denny Way/Lake Union CSO Project. October 1997. Available from Washington State Department of Natural Resources Washington Geologic Information Portal, last accessed May 10, 2022.
- Shannon & Wilson, Inc. (1997) Geotechnical Report Terminal 18 Project Off-Terminal Improvements Harbor Island, Seattle, Washington. November 1997. Available from Washington State Department of Natural Resources Washington Geologic Information Portal, last accessed May 26, 2022.
- Shannon & Wilson, Inc. (1998) *Geotechnical Report, West Galer Street Ramp, Seattle, Washington*. June 1998. Available from Washington State Department of Natural Resources Washington Geologic Information Portal, last accessed May 10, 2022.
- Sideras S (2019) Evolutionary intensity measures for more accurate and informative evaluation of liquefaction triggering. PhD Dissertation, University of Washington, Seattle, WA
- Stephenson WJ, Reitman NG, and Angster SJ (2017) *P-and S-wave velocity models incorporating the Cascadia subduction zone for 3D earthquake ground motion simulations, Version 1.6*—Update for Open-File Report 2007–1348 (No. 2017-1152). United States Geological Survey.
- Terra Associates, Inc. (2000) Geotechnical Report Adams News Building Renovation 1555 West Galer Street Seattle, Washington. March 10, 2000. Available from Washington State Department of Natural Resources Washington Geologic Information Portal, last accessed May 10, 2022.
- Terra Associates, Inc. (2000) Report Geotechnical Engineering Services Proposed Water System Improvements King County International Airport Seattle and Tukwila, Washington. April 6, 2001.

- Rasanen RA, Geyin M, Maurer BW. Select liquefaction case histories from the 2001 Nisqually, Washington, earthquake: A digital data set and assessment of model performance. Earthquake Spectra. 2023;0(0). doi:10.1177/87552930231174244
- Available from Washington State Department of Natural Resources Washington Geologic Information Portal, last accessed June 11, 2022.
- Upadhyaya S, Green RA, Rodriguez-Marek A, Maurer BW, Wotherspoon L, Bradley BA and Cubrinovski M (2019) Influence of corrections to recorded peak ground accelerations due to liquefaction on predicted liquefaction response during the 2010-2011 Canterbury, New Zealand, earthquake sequence. In *Proc.* 13th Australia New Zealand Conference on Geomechanics (13ANZCG).
- van Ballegooy S, Malan P, Lacrosse V, Jacka ME, Cubrinovski M, Bray JD, O'Rourke TD, Crawford SA and Cowan H (2014a) Assessment of liquefaction-induced land damage for residential Christchurch. *Earthquake Spectra* 30(1): 31-55.
- Walsh, TJ (2001). Working a geologic disaster. Washington Geology 28(3): 6-18.
- Washington Division of Geology and Earth Resources (2016) Surface geology, 1:100,000--GIS data, November 2016: Digital Data Series DS-18, version 3.1, previously released June 2010
- Whitman RV (1971) Resistance of soil to liquefaction and settlement. *Soils and Foundations*, 11(4): 59-68.
- Wirth EA, Chang SW, and Frankel AD (2018) 2018 report on incorporating sedimentary basin response into the design of tall buildings in Seattle, Washington. US Geol. Surv. Open-File Rept. 2018-1149.
- Wong IG, Stokoe KH, Cox BR, Lin YC, and Menq FY (2011) Shear-wave velocity profiling of strong motion sites that recorded the 2001 Nisqually, Washington, earthquake. *Earthquake Spectra*, 27(1)" 183-212.
- Wu Q, Li DQ, and Du W (2022) Identification of optimal ground-motion intensity measures for assessing liquefaction triggering and lateral displacement of liquefiable sloping grounds. *Earthquake Spectra*: 87552930221094344.
- Zhu J, Baise LG, and Thompson EM (2017) An updated geospatial liquefaction model for global application. *Bulletin of the Seismological Society of America*, 107(3): 1365-1385.
- Zipper Zeman Associates, Inc. (2002) Geotechnical Engineering Design Study Bush School Project Phase 1 Seattle, Washington. June 28, 2002. Available from Washington State Department of Natural Resources Washington Geologic Information Portal, last accessed May 10, 2022.